Journal of Theoretical Biology ■ (■■■■) ■■■–■■■

Contents lists available at ScienceDirect

Journal of Theoretical Biology

journal homepage: www.elsevier.com/locate/yjtbi

Mathematical model for alopecia areata

Atanaska Dobreva [a,*], Ralf Paus [b,c], N.G. Cogan [a]

[a] Department of Mathematics, 208 Love Building, 1017 Academic Way, Florida State University, Tallahassee, FL 32306, USA
[b] Laboratory for Hair Research and Regenerative Medicine, Department of Dermatology, University of Münster, Münster, Germany
[c] Institute of Inflammation and Repair, University of Manchester, Manchester, UK

HIGHLIGHTS

- We develop a model to explore the dynamics of alopecia areata (AA).
- The model reflects interactions between hair follicles and the immune system.
- Interferon-γ and immune privilege guardians govern disease development and recovery.
- Our results agree with the immune privilege collapse hypothesis for AA pathogenesis.

ARTICLE INFO

Article history:
Received 13 December 2014
Received in revised form
14 May 2015
Accepted 21 May 2015

Keywords:
Autoimmunity
Immune privilege
Hair loss

ABSTRACT

Alopecia areata (AA) is an autoimmune disease, and its clinical phenotype is characterized by the formation of distinct hairless patterns on the scalp or other parts of the body. In most cases hair falls out in round patches. A well-established hypothesis for the pathogenesis of AA states that collapse of hair follicle immune privilege is one of the essential elements in disease development. To investigate the dynamics of alopecia areata, we develop a mathematical model that incorporates immune system components and hair follicle immune privilege agents whose involvement in AA has been confirmed in studies and experiments. We perform parameter sensitivity analysis in order to determine which inputs have the greatest effect on outcome variables. Our findings suggest that, among all processes reflected in the model, immune privilege guardians and the pro-inflammatory cytokine interferon-γ govern disease dynamics. These results agree with the immune privilege collapse hypothesis for the development of AA.

1. Introduction

Alopecia areata (AA) is a noncontagious disease which causes loss of hair on the scalp or other parts of the body. Males and females of different ages and ethnicities can be affected, and about 2% of the U.S. population suffers from the disease (Gilhar et al., 2012). Alopecia areata causes frustration for patients and negatively impacts their social lives (Kalabokes, 2011). The most common clinical presentation is patchy alopecia characterized by the formation of round or oval hairless lesions (Gilhar et al., 2012; Alkhalifah et al., 2010a). In the majority of cases hair loss is not permanent, and there is a potential for regrowth. However, at present there is no cure or preventative measure for AA. Existing remedies have only temporary effect, so when treatment is discontinued relapse is very frequently observed. Also, there is no universally accepted remedy that would work for every patient which often makes disease management problematic. Immunosuppressants are most frequently used to treat the disease, and these can be given in the form of pills, injections, or ointments (Gilhar et al., 2012; Alkhalifah et al., 2010b; Kutner and Friedman, 2013). When such remedies fail to be effective, there are patients who even try treatments from alternative medicine such as acupuncture, rubbing lesions with garlic and herbs, or taking vitamin supplements (Hajheydari et al., 2007). In some cases, spontaneous recovery could also occur (Gilhar et al., 2012).

There has been controversy as to what causes AA. Prevalent hypothesis is that AA is an autoimmune disease, so hair loss occurs due to an immune system response directed against autoantigens synthesized in hair follicles (Giordano and Sinha, 2013; McElwee et al., 2013). In producing hair, follicles go through a natural constantly repeating cycle comprising three phases: anagen (growth phase), catagen (regression phase), and telogen (resting phase), and AA interrupts the growth phase (Gilhar et al., 2007; Ito et al., 2004). In addition, hair follicles are among the body sites that enjoy immune privilege, so normally hair follicles are protected from immune system attacks (Gilhar, 2010; Ito, 2010). Because of this reason, it is believed that the pathogenesis of AA involves collapse of hair follicle immune privilege (McElwee et al.,

* Corresponding author. Tel.: +1 571 224 6448.
E-mail address: adobreva@math.fsu.edu (A. Dobreva).

http://dx.doi.org/10.1016/j.jtbi.2015.05.033
0022-5193/

2013; Ito et al., 2004; Paus et al., 1994). However, the interactions and events occurring during disease onset as well as during relapse and remission are still not completely elucidated (McElwee et al., 2013).

Genetic factors associated with AA have been explored through a computational model (Catanzaro et al., 2010), and the hair cycle has been simulated with a cellular automata model (Halloy et al., 2000, 2002) as well as ordinary differential equations (Al-Nuaimi et al., 2012) and stochastic differential equations (Murray et al., 2012). While these models capture important characteristics of the disease, namely, genetic predisposition, circular lesion pattern, and hair cycle disruption, they do not provide an insight into the interactions between hair follicles and the immune system. Also, some mathematical models exist for animal autoimmune conditions that damage immune-privileged sites, such as experimental autoimmune uveoretinitis, which affects the eye (Nicholson et al., 2012), and experimental autoimmune encephalomyelitis, which affects the brain (Borghans et al., 1998). However, to our knowledge, there have not been previous attempts to mathematically model an autoimmune reaction in the hair follicle environment. This is why, to aid in the effort of better understanding AA development and recovery, we construct a mathematical model that includes immune system constituents and hair follicle immune privilege agents.

The structure of our study is as follows. Section 2 discusses immune privilege of hair follicles and presents the immune privilege collapse hypothesis for disease pathogenesis. We also elaborate on the hair growth cycle, and how it is affected by AA. Section 3 first presents the conceptual formulation of our mathematical model. Then, in Section 3.1, we introduce the full system of equations, and in Section 3.2, we reduce the model in order to make it simpler to analyze. In Section 3, we explore the qualitative behavior of the reduced model through simulations, parameter sensitivity analysis, and linear stability and bifurcation analysis. Finally, Section 4 concludes the paper with a discussion of our findings, and how they pertain to treatment strategies for AA.

2. Alopecia areata and immune privilege

Immune privilege (IP) is a temporary state established only when follicles make pigmented hair because this is when autoantigens are produced (Gilhar et al., 2012; Ito, 2010). Furthermore, IP is restricted to the follicle's lower part which is called hair bulb and constitutes the hair production and pigmentation machinery (Paus et al., 2005). Immune privilege is established and maintained through the secretion of immune privilege guardians such as transforming growth factor-β (TGF-β) and α-melanocyte-stimulating hormone (α-MSH) (Ito et al., 2004; Ito, 2010; Paus et al., 2003). These immunosuppressive substances, synthesized in hair follicles, downregulate the expression of MHC class I molecules in the hair bulb and inhibit lymphocyte accumulation and activation (McElwee et al., 2013; Ito et al., 2004; Paus et al., 2005, 2008). So, IP serves to prevent the immune system from recognizing autoantigens made in the hair bulb during hair production and pigmentation (Gilhar et al., 2007). An AA-affected follicle loses its immune privilege, and as a result its hair bulb becomes MHC class I-positive. Also, a significant amount of leukocytes migrate to the diseased hair follicle (Gilhar et al., 2007; McElwee et al., 2003, 2002).

Hair follicles are organs that constantly cycle throughout a person's life (Al-Nuaimi et al., 2012, 2010; Paus and Cotsarelis, 1999; Millar, 2002). Alopecia areata disrupts this natural cycle, but it does not cause damage to hair follicles' structure, so affected follicles do not lose their capability to produce hair (Gilhar et al., 2012, 2007). The hair follicle cycle has three stages: anagen, catagen, and telogen (Al-Nuaimi et al., 2012, 2010; Paus and Cotsarelis, 1999). Anagen is the active growth phase during which pigmented hair is produced. During catagen, hair growth stops, and the follicle shrinks due to apoptosis of its bulb keratinocytes. Throughout telogen, the hair follicle is dormant. Production of a new hair shaft commences at the end of telogen, and as this new fiber grows, the old one is pushed out of the hair canal and discarded (Al-Nuaimi et al., 2012, 2010; Paus and Cotsarelis, 1999). The three cycle phases have different lengths on average: anagen lasts 2–5 years, catagen 3–6 weeks, and telogen 3–5 months (Al-Nuaimi et al., 2012; Bergfeld and Mulinari-Brenner, 2001). Almost always, hair follicles get affected by AA when they are in anagen. The infiltrates of leukocytes observed in diseased hair follicles cause these follicles to exit anagen much earlier than normal and enter catagen. On the other hand, AA does not interfere with the lengths of catagen and telogen. After affected hair follicles exit anagen prematurely and go through catagen and telogen, they could re-enter the growth stage. However, if by that time immune privilege has not been restored, anagen would again have significantly shortened duration (Gilhar et al., 2007).

The pro-inflammatory cytokine interferon-γ (IFN-γ) plays a crucial role in the premature termination of anagen and consequent induction of catagen (Freyschmidt-Paul et al., 2006; Ito et al., 2005). Evidence from experiments also shows that autoreactive $CD4^+$ and $CD8^+$ T-cells/$NKG2D^+$ cells are involved in the pathogenesis of AA, and that hair loss results from cooperative activities of these lymphocytes (Gilhar et al., 1998, 2002, 2007; Freyschmidt-Paul et al., 2006). According to the hair follicle immune privilege collapse hypothesis of Paus et al. (2003), disease development is characterized by overlap of the following key events:

1. Hair follicles enter the anagen phase of the hair cycle during which pigmented hair is produced.
2. Due to some external factors, such as stress, local injury, or inflection, IFN-γ secretion is increased, and this induces collapse of immune privilege of anagen hair follicles.
3. The loss of immune privilege results in MHC class I expression in the hair bulb. In a healthy hair follicle, MHC class I molecules are either absent, or their expression is very low.
4. MHC class I expression in the hair bulb promotes autoantigen presentation to autoreactive $CD8^+$ T-cells/$NKG2D^+$ cells.
5. Autoreactive $CD8^+$ T-cells/$NKG2D^+$ cells, assisted by $CD4^+$ T-cells, attack the epithelium of anagen hair follicles, and this results in premature termination of the growth phase and subsequent shedding of hair fibers (Gilhar et al., 2012, 2007; Paus et al., 1994, 2003).

In addition, the hypothesis states that sufficient amount of potent immune privilege guardians can inhibit IFN-γ secretion, suppress MHC class I expression, and restore hair follicle immune privilege (Gilhar et al., 2012, 2007; Paus et al., 2003).

3. Mathematical model

In order to study how alopecia areata (AA) develops over time, we construct a mathematical model which includes the dynamics of immune system constituents and hair follicle immune privilege agents. We consider a small cluster of hair follicles and assume that they are in the anagen phase of the hair growth cycle. This assumption allows us to focus on the interactions between hair follicles and immune system components, which is a very important initial step in understanding the temporal disease dynamics. In addition, we assume that hair follicles are homogeneous. Fig. 1 shows the conceptual formulation of the model, which is as follows:

Please cite this article as: Dobreva, A., et al., Mathematical model for alopecia areata. J. Theor. Biol. (2015), http://dx.doi.org/10.1016/j.jtbi.2015.05.033

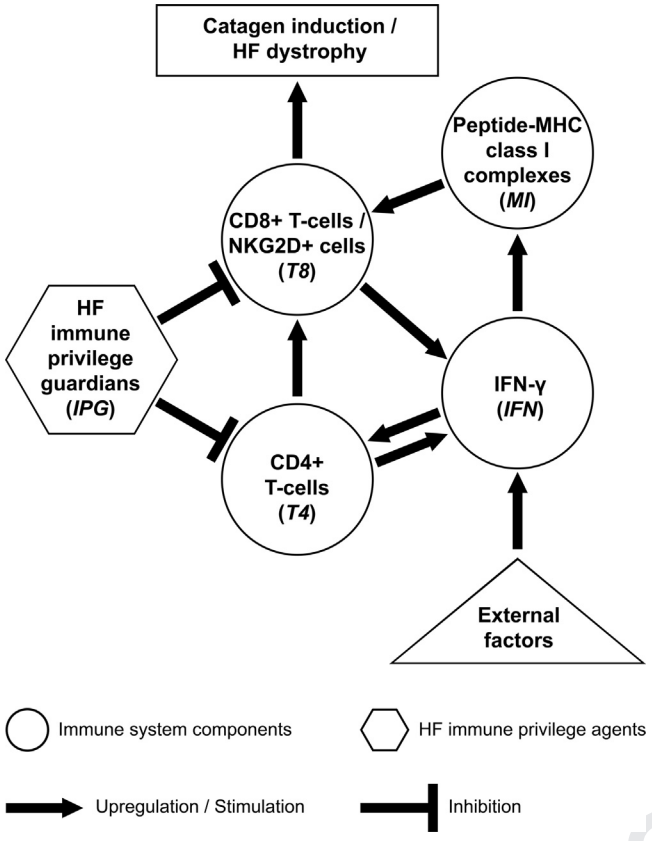

Fig. 1. Model diagram. External factors cause elevated production of IFN-γ (*IFN*) in the hair follicle (HF) environment. IFN-γ upregulates MHC I expression which leads to increased formation of complexes of autoantigen-derived peptides bound to MHC I molecules (*MI*). These pro-inflammatory signals trigger the migration of $CD4^+$ and $CD8^+$ T-cells/$NKG2D^+$ cells to hair follicles. $CD4^+$ T-cells get activated in response to IFN-γ and become effector cells which then proliferate. $CD8^+$ T-cells/$NKG2D^+$ cells get activated as they recognize peptide-MHC I complexes, and to undergo clonal expansion, the effector cells need co-stimulatory signals/proliferation stimuli from $CD4^+$ T-cells. Activated $CD4^+$ T-cells (*T4*) and $CD8^+$ T-cells/$NKG2D^+$ cells (*T8*) produce IFN-γ. Effector autoreactive $CD8^+$ T-cells/$NKG2D^+$ cells that accumulate in the hair follicle attack the anagen hair bulb, which results in premature catagen induction. The activation and clonal expansion of $CD4^+$ and $CD8^+$ T-cells/$NKG2D^+$ cells are inhibited by immune privilege guardians (*IPG*).

- External factors such as infection or stress lead to increased production of IFN-γ (*IFN*) in the hair follicle environment which opens up a cross-talk between a small cluster of hair follicles and the immune system.
- IFN-γ upregulates MHC I expression in the hair bulb, and this promotes autoantigen presentation through increased formation of peptide–MHC I complexes (*MI*) on the surface of hair matrix keratinocytes.
- In response to the pro-inflammatory signals, $CD4^+$ T-cells and $CD8^+$ T-cells/$NKG2D^+$ cells migrate to hair follicles. When these lymphocytes first reach a hair follicle, they are resting cells which need to get activated and become effector cells.
- IFN-γ helps to activate $CD4^+$ T-cells and turn them into effector cells which then proliferate.
- $CD8^+$ T-cells/$NKG2D^+$ cells get activated in response to peptide-MHC I complexes, and to undergo clonal expansion the effector cells receive help from $CD4^+$ T-cells in the form of proliferation stimuli/co-stimulatory signals.
- Activated $CD4^+$ T-cells (*T4*) and $CD8^+$ T-cells/$NKG2D^+$ cells (*T8*) produce IFN-γ, which maintains the pro-inflammatory environment and keeps the cycle running.
- The large amounts of effector autoreactive $CD8^+$ T-cells/$NKG2D^+$ cells that accumulate in the hair follicle launch a cytotoxic attack on the anagen hair bulb. As a result, hair growth and pigmentation are prematurely stopped, and the hair follicle is pushed into catagen, the regression stage of the hair cycle.
- Activation and proliferation of $CD4^+$ T-cells and $CD8^+$ T-cells/$NKG2D^+$ cells are inhibited by immune privilege guardians (*IPG*) produced in hair follicles. Sufficient amount of these immunosuppressive substances can terminate the pro-inflammatory cycle and restore immune privilege (Gilhar et al., 2012, 2007; Ito et al., 2004; Paus et al., 2003; Sun et al., 2008).

3.1. Model construction

1. *Assumption*: Hair follicles are in the anagen phase of the hair growth cycle.
2. Model variables:
   - *IPG*: amount of immune privilege guardians.
   - *IFN*: amount of IFN-γ.
   - *MI*: amount of peptide-MHC class I complexes.
   - *T8*: population of effector autoreactive $CD8^+$ T-cells/$NKG2D^+$ cells.
   - *T4*: population of effector autoreactive helper $CD4^+$ T-cells.

   All of the above constituents are localized to the small cluster of hair follicles considered.
3. *Equations*: We model the dynamics of immune privilege guardians, IFN-γ, and peptide-MHC class I complexes with equations whose general structure is

$$\frac{d*}{dt} = Production - Degradation.$$

Immune privilege guardians are produced at a constant rate (p_{IPG}), and their amount decreases due to natural degradation ($-d_{IPG}IPG$). IFN-γ is secreted by effector $CD4^+$ and $CD8^+$ T-cells/$NKG2D^+$ cells ($p_{IFN}T4 + p_{IFN}T8$), and natural degradation causes the IFN-γ level to decline ($-d_{IFN}IFN$). The amount of peptide-MHC class I complexes increases due to increase in the production of IFN-γ and is saturating in IFN-γ $\left(p_{MI}\frac{IFN}{\tau + IFN}\right)$ (Yang et al., 2004). Peptide–MHC class I complexes are also subject to natural decay ($-d_{MI}MI$).

The equations used to describe the dynamics of effector $CD4^+$ and $CD8^+$ T-cells/$NKG2D^+$ cells follow the general structure

$$\frac{d*}{dt} = Migration\&Activation + Proliferation - Death.$$

Autoreactive $CD8^+$ T-cells/$NKG2D^+$ cells migrate into hair follicles, get activated as they recognize complexes of autoantigen-derived peptides bound to MHC class I molecules, and activation is inhibited by immune privilege guardians $\left(m_{T8}\frac{\alpha MI}{1+\sigma IPG}\right)$. The clonal expansion of effector $CD8^+$ T-cells/$NKG2D^+$ cells is promoted by co-stimuatory and cell division signals provided by $CD4^+$ T-cells, and proliferation is hindered by immune privilege guardians $\left(\frac{p_{T8}\gamma T4 T8}{1+\sigma IPG}\right)$. The $CD8^+$ T-cell/$NKG2D^+$ cell population decreases due to natural cell death ($-d_{T8}T8$), and if the population size is significantly large, there is also death associated with competition among $CD8^+$ T-cells/$NKG2D^+$ cells ($-\kappa_{T8}(T8)^2$) (Borghans et al., 1998; Yates et al., 2000; Segel et al., 1995).

Autoreactive $CD4^+$ T-cells migrate to hair follicles, and activation of these cells is stimulated by IFN-γ and inhibited by immune privilege guardians $\left(m_{T4}\frac{\beta IFN}{1+\sigma IPG}\right)$. The immune privilege agents also

inhibit CD4$^+$ T-cell proliferation $\left(\frac{p_{T4}T4}{1+\sigma IPG}\right)$. The CD4$^+$ T-cell population declines as CD4$^+$ T-cells undergo natural death ($-d_{T4}T4$) or die because of inter-cell competition ($-\kappa_{T4}(T4)^2$) (Borghans et al., 1998; Yates et al., 2000; Segel et al., 1995).

As noted earlier, AA-affected hair follicles experience hair cycle disruption: premature termination of anagen and induction of catagen. The large populations of effector autoreactive CD4$^+$ T-cells and CD8$^+$ T-cells/NKG2D$^+$ cells bring about the destruction of anagen hair bulb keratinocytes. As a result, hair follicles are unable to sustain the process of hair growth and pigmentation, and they enter the hair cycle regression stage (Gilhar et al., 2012, 2007). So, an inverse relationship exists between the amount of hair bulb keratinocytes (H) and the amount of CD4$^+$ and CD8$^+$ T-cells/NKG2D$^+$ cells ($T=T4+T8$). As shown in Fig. 2, a phenomenological description of this relationship between H and T could be formulated as follows:

$$H(T)=\eta_1-\frac{\eta_1}{1+e^{-T+\eta_2}}. \tag{1}$$

When T is close to zero, H is maintained at a high level signifying hair production. When T becomes large, H decreases rapidly toward zero indicating that hair growth slows down and stops. We should note that $H(T)$ is only meant to convey qualitative relationships and is not meant to be quantitative or definitive.

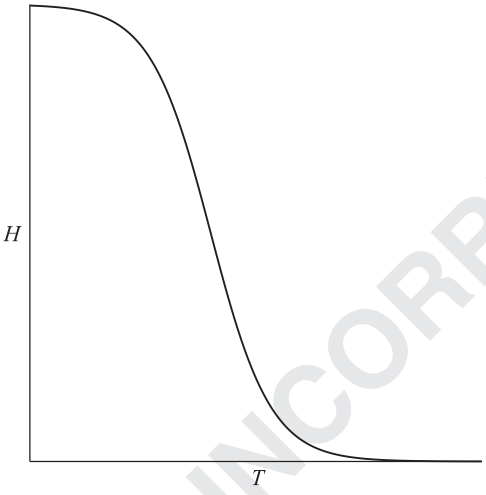

Fig. 2. Graphical representation of catagen induction. The amount of hair bulb cells, H, is inversely related to the amount of CD4$^+$ and CD8$^+$ T-cells/NKG2D$^+$ cells, T ($T=T4+T8$). A sample mathematical formulation of this inverse relationship between H and T is given by $H(T)=\eta_1-\frac{\eta_1}{1+e^{-T+\eta_2}}$.

The following system of equations constitutes the full mathematical model, and it captures the interactions and events discussed above

$$\frac{dIPG}{dt}=p_{IPG}-d_{IPG}IPG \tag{2}$$

$$\frac{dIFN}{dt}=p_{IFN}T4+p_{IFN}T8-d_{IFN}IFN \tag{3}$$

$$\frac{dMI}{dt}=p_{MI}\frac{IFN}{r+IFN}-d_{MI}MI \tag{4}$$

$$\frac{dT8}{dt}=m_{T8}\frac{\alpha MI}{1+\sigma IPG}+\frac{p_{T8}\gamma T4T8}{1+\sigma IPG}-d_{T8}T8-\kappa_{T8}(T8)^2 \tag{5}$$

$$\frac{dT4}{dt}=m_{T4}\frac{\beta IFN}{1+\sigma IPG}+\frac{p_{T4}T4}{1+\sigma IPG}-d_{T4}T4-\kappa_{T4}(T4)^2 \tag{6}$$

$$H(T)=\eta_1-\frac{\eta_1}{1+e^{-T+\eta_2}},\quad T=T8+T4. \tag{7}$$

3.2. Model reduction

Alopecia areata development involves processes which happen at different time scales. The time courses of cytokine secretion, receptor binding and degradation are on the order of minutes, while lymphocyte migration, activation, proliferation, and death occur on the order of days (Yates et al., 2000; Lortat-Jacob et al., 1996; Akdis et al., 1995; Ashton et al., 1977; Kirschner, 1999; Mohri et al., 2001; Schiller et al., 2004). Similarly, the rates of peptide–MHC I complex formation, receptor binding, and decay are much larger compared to the rates associated with changes in the lymphocyte populations (Mohri et al., 2001; Princiotta et al., 2003; Ackerman and Cresswell, 2003). Because *IPG*, *IFN*, and *MI* have faster dynamics, no changes in these quantities can be detected on the time scale of cell dynamics. This allows us to assume that *IPG*, *IFN*, and *MI* remain constant, so we set $\frac{dIPG}{dt}=0$, $\frac{dIFN}{dt}=0$, and $\frac{dMI}{dt}=0$. For simplicity, we also assume that CD4$^+$ and CD8$^+$ T-cells/NKG2D$^+$ cells have comparable rates of migration, proliferation, death, and concentration-dependent death. That is, $m_{T8}=m_{T4}=m$, $p_{T8}=p_{T4}=p$, $d_{T8}=d_{T4}=d$, $\kappa_{T8}=\kappa_{T4}=\kappa$.

Next, we re-scale and use the above assumptions in order to obtain the following simplified model with dimensionless variables and parameters:

$$\frac{dx}{d\tau}=\frac{v(x+y)}{(1+s)(a+y+x)}+\frac{lxy}{(1+s)}-x-x^2 \tag{8}$$

Table 1
Parameters in the full model and their nominal values.

Parameter	Description	Value	Units	Reference
m	Migration rate of $T4$ and $T8$	0.10	ml/day	(Kirschner, 1999; Eicheler et al., 1998)
α	Activation rate of $T8$ in response to *MI*	0.05	(Peptide–MHC I complexes)$^{-1}$	(Schodin et al., 1996; Kageyama et al., 1995)
μ	Ratio of *MI* production rate to *MI* degradation rate	3.2×10^5	Peptide–MHC I complexes	Princiotta et al., 2003; Ackerman and Cresswell, 2003)
σ	*IPG* inhibitory signal strength	1	(ng ml)$^{-1}$	Estimated
c	Ratio of *IPG* production rate to *IPG* degradation rate	3.4×10^{-4}	ng/ml	(Ashton et al., 1977; Schiller et al., 2004)
g	Ratio of *IFN* production rate to *IFN* degradation rate	4.2×10^{-5}	ng/ml	(Lortat-Jacob et al., 1996; Akdis et al., 1995)
r	*MI* half saturation due to *IFN*	10	ng	Estimated
p	Proliferation rate of $T4$ and $T8$	0.004185	day^{-1}	(Mohri et al., 2001) and Estimation
γ	Amount of co-stimulation and proliferation stimuli from $T4$	7.55×10^{-5}	ml^{-1}	Estimated
d	Death rate of $T4$ and $T8$	0.05	day^{-1}	(Mohri et al., 2001) and Estimation
κ	Concentration-dependent death rate of $T4$ and $T8$	5×10^{-7}	(ml day)$^{-1}$	Estimated
β	Activation rate of $T4$ in response to *IFN*	6.25	ng^{-1}	Estimated

Table 2
Parameters in the reduced model and their biological significance.

Parameter	Biological information captured
$s=\sigma c$	Strength of immunosuppression and production to degradation ratio of HF immune privilege guardians
$v=\frac{m\alpha\mu\kappa}{d^2}$	Lymphocyte migration, peptide–MHC I complex formation, activation of $CD8^+$ T-cells, natural and concentration-dependent death rate of lymphocytes
$l=\frac{p\gamma}{\kappa}$	Co-stimulatory and proliferation signals from $CD4^+$ T-cells, proliferation rate and concentration-dependent death rate of lymphocytes
$a=\frac{r\kappa}{gd}$	Production to degradation ratio of IFN-γ, natural and concentration-dependent death rate of lymphocytes, half saturation of peptide-MHC I complex formation due to IFN-γ
$b=\frac{m\beta g}{d}$	Activation of $CD4^+$ T-cells, lymphocyte migration and natural death, production to degradation ratio of IFN-γ
$w=\frac{p}{d}$	Ratio of proliferation rate to natural degradation rate of lymphocytes

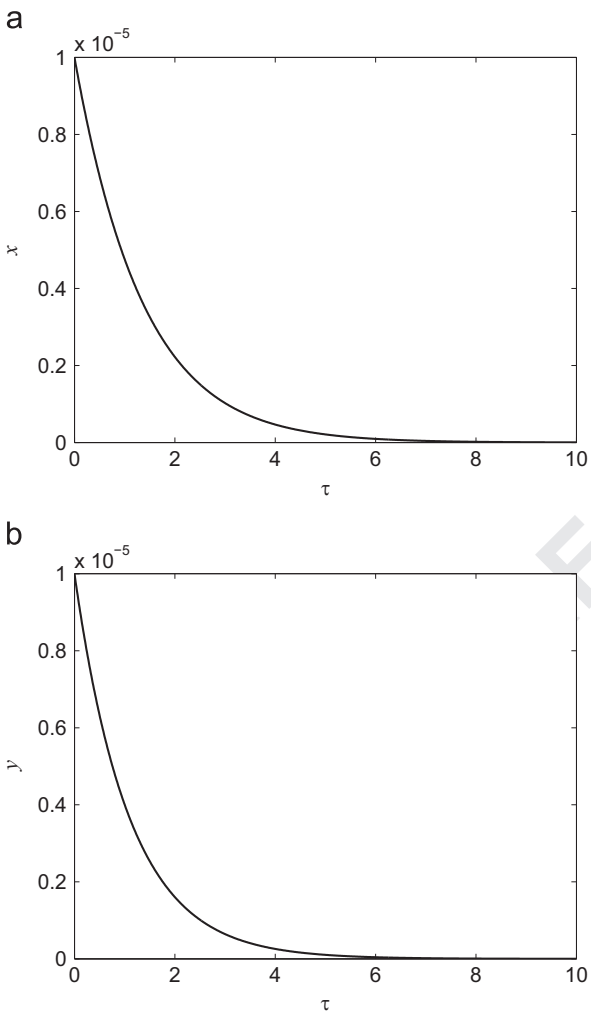

Fig. 3. Healthy state. As initial conditions for this simulation we use $x=10^{-5}$ ($T8=1$ cell) and $y=10^{-5}$ ($T4=1$ cell). The results show that, as time passes, the populations of $CD8^+$ and $CD4^+$ T-cells are quickly brought down to zero, so immune system attacks are prevented from occurring. (a) Time evolution of $CD8^+$ T-cell scaled population size. (b) Time evolution of $CD4^+$ T-cell scaled population size.

$$\frac{dy}{d\tau}=\frac{b(x+y)}{(1+s)}+\frac{wy}{(1+s)}-y-y^2 \tag{9}$$

All parameters in the reduced model are combinations of parameters from the full model. The full model parameters and their nominal levels are listed in Table 1, and the dimensionless parameters are given in Table 2.

To estimate parameters for which we had insufficient information, we fit our model to the following experimental data:

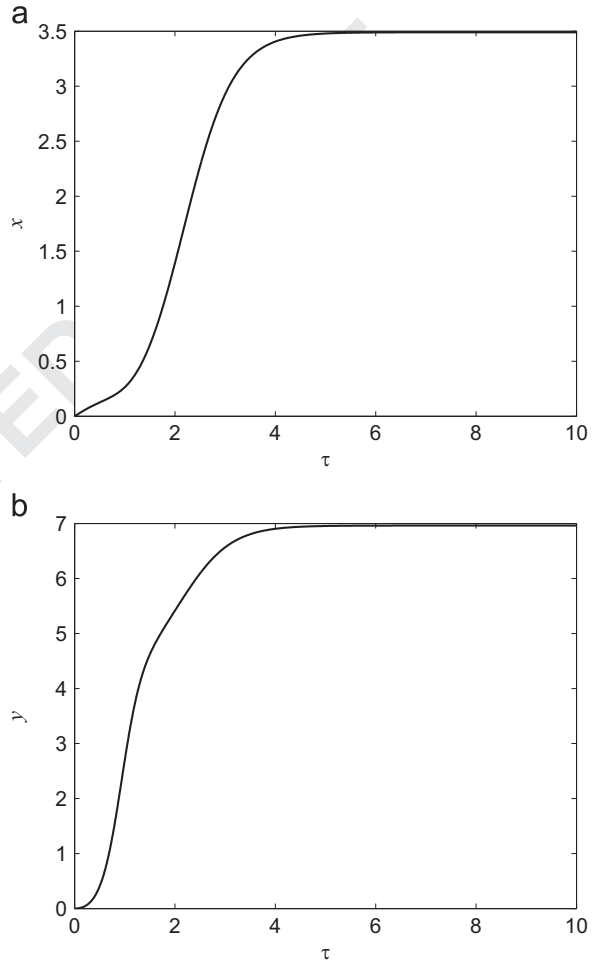

Fig. 4. Diseased state. As initial conditions for this simulation we use $x=10^{-5}$ ($T8=1$ cell) and $y=10^{-5}$ ($T4=1$ cell). The results show that alopecia areata develops in about 100 days ($\tau=5$ corresponds to $t=100$ days). (a) Time evolution of $CD8^+$ T-cell scaled population size. (b) Time evolution of $CD4^+$ T-cell scaled population size.

- A dose of 7.5×10^5 $CD8^+$ T-cells causes AA to develop in mice in 57–69 days (Alli et al., 2012).
- Scalp grafts onto SCID mice exhibit hair loss 68 days after being injected with about 10^6 scalp T-cells incubated in advance with hair follicle homogenate (Gilhar et al., 1998).
- The ratio of number of $CD4^+$ T-cells to number of $CD8^+$ T-cells in the lymphocytic infiltrate is about 2:1 (Ito, 2013; Zhao et al., 2012; Rivitti, 2005).

Also, based on these data we select for $T8$ and $T4$ to be measured in 10^5 *cells*. As part of the model reduction process, presented in more detail in Appendix A, we express the variables $T8$, $T4$, and t as $T8=x\hat{x}$, $T4=y\hat{y}$, $t=\tau\hat{t}$ where x, y, and τ are dimensionless

Please cite this article as: Dobreva, A., et al., Mathematical model for alopecia areata. J. Theor. Biol. (2015), http://dx.doi.org/10.1016/j.jtbi.2015.05.033

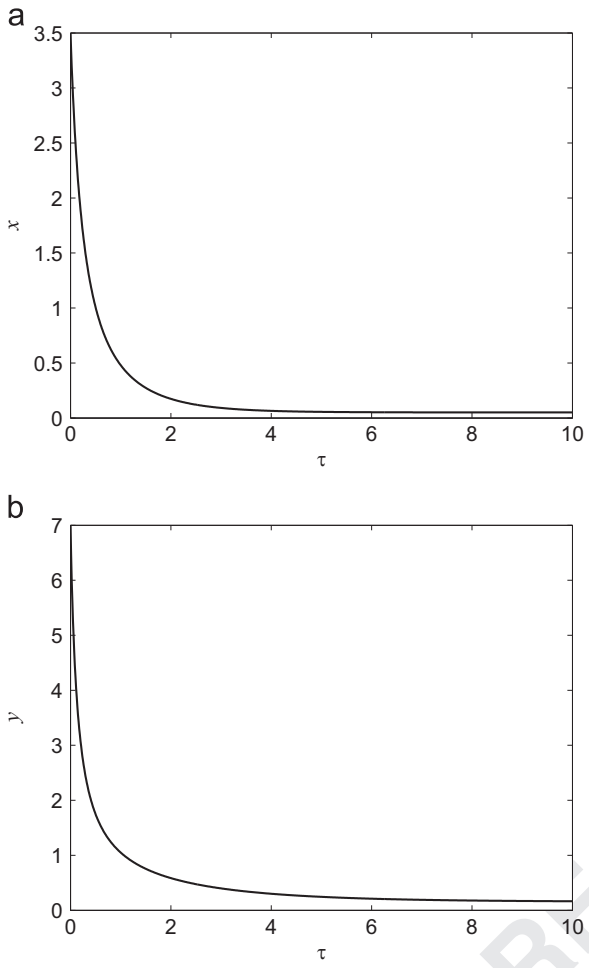

Fig. 5. State of treatment. The initial conditions for this simulation are $x=3.5$ ($T8=3.5\times10^5$ cells) and $y=7$ ($T4=7\times10^5$ cells). The results show that a high enough level of potent immune privilege guardians causes a rapid decrease in the $CD8^+$ and $CD4^+$ T-cell populations leading to recovery from the disease. (a) Time evolution of $CD8^+$ T-cell scaled population size. (b) Time evolution of $CD4^+$ T-cell scaled population size

Table 3
Healthy state, diseased state, and state of treatment: values of full model parameters.

Parameter	Healthy state	Diseased state	State of treatment
m	0.10 ml/day	0.10 ml/day	0.10 ml/day
α	0.05 (pep–MHC I)$^{-1}$	0.05 (pep–MHC I)$^{-1}$	0.05 (pep–MHC I)$^{-1}$
μ	3.2×10^5 pep–MHC I	3.2×10^5 pep–MHC I	3.2×10^5 pep–MHC I
σ	1 (ng ml)$^{-1}$	1 (ng ml)$^{-1}$	15 (ng ml)$^{-1}$
c	0.00034 ng ml	0.00034 ng ml	0.34 ng ml
g	4.2×10^{-5} ng ml	4.2×10^{-1} ng ml	4.2×10^{-1} ng ml
r	10 ng	10 ng	10 ng
p	0.004185 day^{-1}	0.004185 day^{-1}	0.004185 day^{-1}
γ	7.55×10^{-5} ml^{-1}	7.55×10^{-5} ml^{-1}	7.55×10^{-5} ml^{-1}
d	0.05 day^{-1}	0.05 day^{-1}	0.05 day^{-1}
κ	5×10^{-7} (ml day)$^{-1}$	5×10^{-7} (ml day)$^{-1}$	5×10^{-7} (ml day)$^{-1}$
β	6.25 ng^{-1}	6.25 ng^{-1}	6.25 ng^{-1}

variables, and $\hat{x}$, $\hat{y}$, and $\hat{t}$ carry the units associated with $T8$, $T4$, and t, respectively. We choose $\hat{x}=\hat{y}=\frac{d}{\kappa}$ and $\hat{t}=\frac{1}{d}$. t is measured in *days*, and since $d=0.05$, we have $\hat{t}=20$ *days*. In addition, $\hat{x}=\hat{y}=10^5$ *cells* allows us to make the estimate $\kappa=5\times10^{-7}$.

To validate the reduced model, we compared its output with results obtained from running full model simulations. The relative difference between outcomes is on the order of 10^{-4}, which confirms that the simplified model closely approximates the full model. A significant advantage of the reduced model is ease of analysis. Due to this reason, in the following section we apply a number of techniques to explore how the reduced model behaves.

Table 4
Healthy state, diseased state, and state of treatment: values of reduced model parameters.

Dimensionless parameter	Healthy state	Diseased state	State of treatment
$s=\sigma c$	0.00034	0.00034	5.10
$v=(m\alpha\mu\kappa)/d^2$	0.32	0.32	0.32
$l=(p\gamma)/\kappa$	0.6319	0.6319	0.6319
$a=(r\kappa)/(gd)$	2.381	0.0002381	0.0002381
$b=(m\beta g)/d$	0.000525	5.25	5.25
$w=p/d$	0.0837	0.0837	0.0837

4. Analysis

To investigate the qualitative behavior of the simplified model (Eqs. (8) and (9)), we perform simulations, LHS/PRCC sensitivity analysis as well as linear stability and bifurcation analysis. Based on the experimental data described in the previous section, we run the reduced model for $0\le\tau\le10$, which corresponds to a time course of 200 days.

4.1. Simulations

In this section, we show simulations of the simplified model (Eqs. (8) and (9)) using representative parameter sets for three situations: healthy state (Fig. 3), diseased state (Fig. 4), and state of treatment (Fig. 5). All simulation results we describe below are consistent with the experimental data discussed at the end of Section 2 as well as with the immune privilege collapse hypothesis. So, our model is able to capture qualitatively the behavior and interactions underlying AA dynamics.

In the healthy state simulation all parameters are at their nominal levels given in the first columns of Tables 3 and 4, and the results show that $CD8^+$ and $CD4^+$ T-cell populations go to zero with time, so immune system attacks against hair follicles are prevented. Parameter values for the diseased state simulation are given in the second columns of Tables 3 and 4: parameter g is increased to reflect elevated amount of IFN-γ, while all other parameters are kept at their nominal values. Changing g causes the changes seen in the dimensionless parameters a and b. The diseased state simulation results show that significantly increased level of IFN-γ leads to very large amounts of autoreactive lymphocytes, and AA develops in about 100 days. Parameter values for the state of treatment simulation are listed in the third columns of Tables 3 and 4: parameters c and σ are both increased to reflect high amount and inhibitory strength of immune privilege guardians, which causes a change in the dimensionless parameter s; parameter g is kept at its diseased state value, and the remaining parameters stay at nominal level. From the results in Fig. 5 we can conclude that high enough amount of potent immune privilege guardians causes the $CD8^+$ and $CD4^+$ T-cell populations to diminish to very low levels at which a detrimental autoimmune reaction is suppressed.

We use $x=10^{-5}$ ($T8=1$ cell) and $y=10^{-5}$ ($T4=1$ cell) as initial conditions for the healthy state and diseased state simulations in order to represent negligible initial presence of autoreactive lymphocytes. In the treatment simulation, as initial conditions we use $x=3.5$ ($T8=3.5\times10^5$ cells) and $y=7$ ($T4=7\times10^5$ cells) because these are the levels that $CD8^+$ and $CD4^+$ T-cell populations reach in a state of disease.

Table 5
Parameter ranges and baseline values used in LHS/PRCC analysis.

Parameter	Range	Baseline value
$s=\sigma c$	[0.0003, 5.5]	0.00034
$v=(m\alpha\mu\kappa)/d^2$	[0.11, 0.55]	0.32
$l=(p\gamma)/\kappa$	[0.005, 1.25]	0.6319
$a=(r\kappa)/(gd)$	[0.0002, 2.5]	2.381
$b=(m\beta g)/d$	[0.0005, 5.5]	0.000525
$w=p/d$	[0.055, 0.11]	0.0837

4.2. LHS/PRCC sensitivity analysis

We also perform LHS/PRCC (Latin Hypercube Sampling/Partial Rank Correlation Coefficient) sensitivity analysis in order to investigate the model's behavior and to determine which parameters have the greatest impact on the output. This helps to reduce the model parameter set to explore as well as point to useful clinical targets. We should note here that in sensitivity analysis literature model parameters are also referred to as input variables. LHS/PRCC is one of the several global methods used to conduct sensitivity analysis. Partial rank correlation coefficients quantify the sensitivity of nonlinear monotonic relationships between the parameters and the model outcome. In other words, PRCC is a way to measure how strong the association is between alterations in a parameter and changes in the output (Marino et al., 2008; Blower and Dowlatabadi, 1994). Examples of other global sensitivity analysis techniques are the Sobol method and Fourier Amplitude Sensitivity Test (FAST). In contrast to LHS/PRCC, these methods can be applied in the case of nonlinear non-monotonic relationships between input variables and the model outcome. However, the LHS/PRCC approach is computationally less expensive and simpler to implement (Marino et al., 2008; Blower and Dowlatabadi, 1994).

The LHS/PRCC analysis procedure has two main parts. First, Latin Hypercube Sampling (LHS) design is used to obtain an array of sample values for each parameter. In order to perform this step, probability density functions need to be specified for all parameters (Marino et al., 2008; Blower and Dowlatabadi, 1994). Due to lack of information about the underlying distributions of the parameters in our simplified model, we assign a uniform distribution to every parameter. In doing so, we specify the ranges over which parameters vary. Since we did not have sufficient experimental data available to determine minimum and maximum values for these intervals, we needed to also rely on model estimations. Parameter ranges along with baseline values are listed in Table 5.

The parameter distributions are sampled independently by subdividing the given ranges into non-overlapping regions of equal probability and drawing at random and without replacement a value from each region (Marino et al., 2008; Blower and Dowlatabadi, 1994). Once an array of sample values for each parameter is obtained, these values are used to perform model simulations. The number of simulations depends on how many uncertain parameters there are, and one needs to have $N > \frac{4}{3}K$, where N is the number of simulations, and K is the number of parameters (Blower and Dowlatabadi, 1994). For our model $K=6$, and we set $N=100$. The outcomes of all simulations are stored and subsequently used to implement the second part of the sensitivity analysis procedure, which is calculating a partial rank correlation coefficient (PRCC) for each parameter in the model.

As mentioned above, PRCC quantifies the sensitivity of nonlinear monotonic relationships between the parameters and the model output (Marino et al., 2008; Blower and Dowlatabadi, 1994). We generated scatter plots of the outcome variables against each parameter in order to verify that the monotonicity condition holds; these plots are shown in Appendix B. PRCC values carry two pieces of information. Their magnitude indicates how strong of an impact a parameter has on the outcome. When a PRCC value has magnitude greater than 0.5, the output variable is considered sensitive to changes in the corresponding parameter (Marino et al., 2008). PRCC's sign shows whether the input–output relationship is direct or inverse. A negative PRCC value means that the input and the output move in opposite directions, so as a parameter increases, the output decreases. On the other hand, a positive coefficient means that the input and the output move in the same direction, so an increase in a parameter value leads to an increase in the output (Marino et al., 2008; Blower and Dowlatabadi, 1994).

Table 6
Partial rank correlation coefficient (PRCC) values. (a) Outcome variable: x (scaled level of $CD8^+$ T-cells). (b) Outcome variable: y (scaled level of $CD4^+$ T-cells).

Parameter	PRCC
s	−0.8706*
v	0.3809*
l	−0.0906
a	−0.6973*
b	0.8725*
w	−0.0428

Parameter	PRCC
s	−0.8665*
v	0.1437
l	−0.0370
a	−0.4979*
b	0.8763*
w	0.1280

Results labeled with
* Significant at the 0.001 level.

The LHS/PRCC analysis results, presented in Table 6 and Fig. 6, show that the level of $CD8^+$ T-cells (x) is sensitive to changes in the parameters s, a, and b, and the level of $CD4^+$ T-cells (y) is sensitive to changes in the parameters s and b. Also, the PRCC between a and y has magnitude that is close to the cutoff value of 0.5. $s=\sigma c$ captures the effects of immune privilege guardians. As explained in Table 1, c is the ratio of production rate to degradation rate of immune privilege guardians, and σ is their inhibitory signal strength. On the other hand, the impact of IFN-γ is embedded in $b=\frac{m\beta g}{d}$ and $a=\frac{r\kappa}{gd}$ through the value of g, the ratio of production rate to degradation rate of IFN-γ. These results suggest that the two most important processes in AA dynamics are IFN-γ and hair follicle immune privilege guardians, so disease development and recovery are driven by the interplay between these constituents.

Apart from reflecting the effects of IFN-γ, b also carries information about activation of $CD4^+$ T-cells as well as lymphocyte migration and natural death. In addition, the parameter a incorporates information about natural and concentration-dependent death rate of lymphocytes as well as saturation of peptide–MHC I complex formation due to IFN-γ. However, in the simulations presented earlier variation in b and a is triggered by only changing g, the production to degradation ratio of IFN-γ. Also, the simulations were used as a basis for specifying minimum and maximum values for b and a in the LHS/PRCC analysis. This is why, we conclude that sensitivity of the model outcome to variation in the input parameter b means sensitivity toward changes in the IFN-γ level.

As explained earlier, hair follicles in the diseased state suffer dystrophy and premature catagen induction, and these damaging events are brought about by the large accumulations of effector

Please cite this article as: Dobreva, A., et al., Mathematical model for alopecia areata. J. Theor. Biol. (2015), http://dx.doi.org/10.1016/j.jtbi.2015.05.033

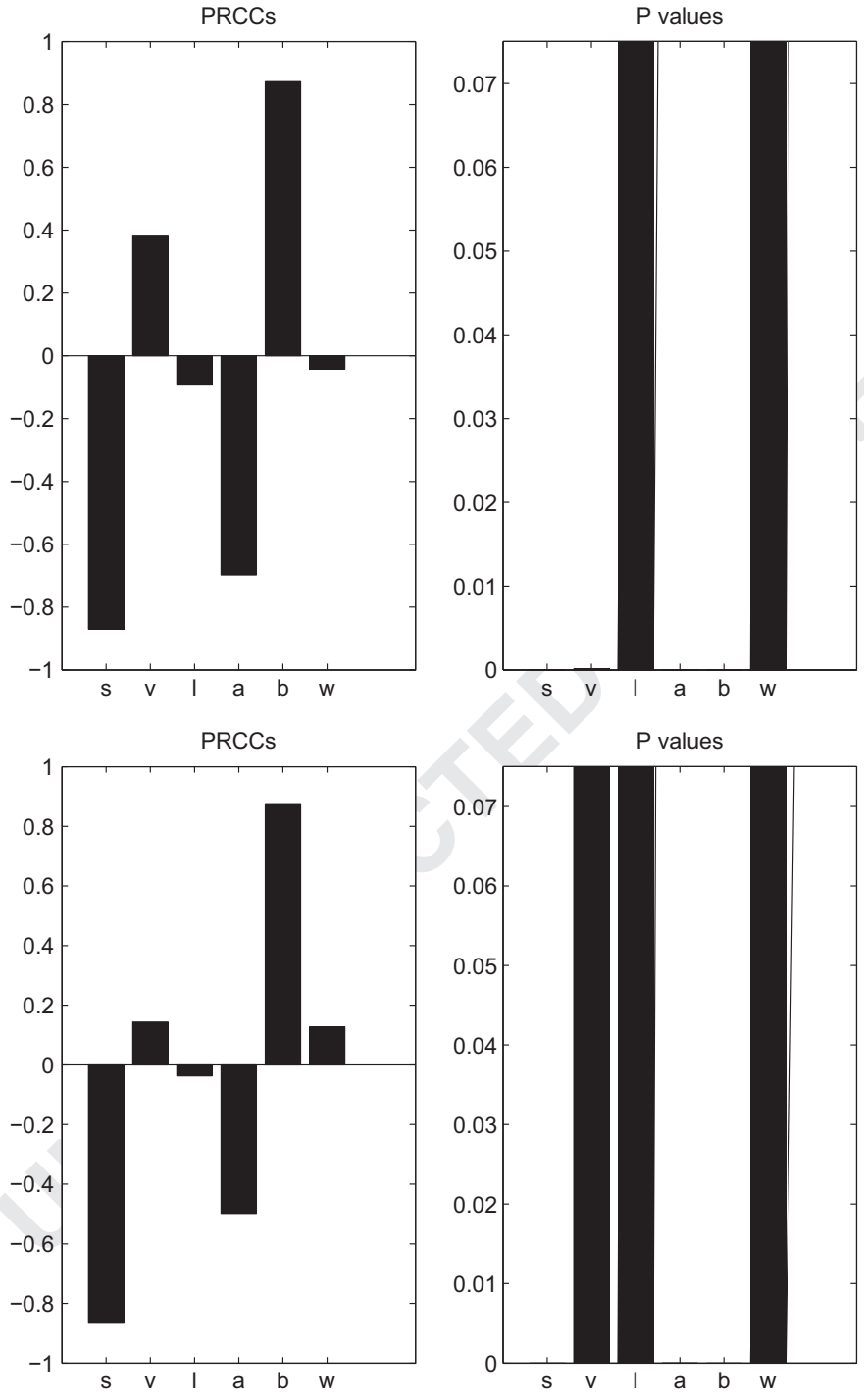

Fig. 6. Graphical representation of LHS/PRCC sensitivity analysis results. The program we used to perform the LHS/PRCC sensitivity analysis was adapted from Matlab code available at http://malthus.micro.med.umich.edu/lab/usanalysis.html (Marino et al., 2008). (a) Outcome: Scaled level of $CD8^+$ T-cells. (b) Outcome: Scaled level of $CD4^+$ T-cells.

autoreactive $CD4^+$ and $CD8^+$ T-cells. The parameter sensitivity analysis, conducted in this section, indicates that the amounts of IFN-γ and immunosuppressive agents influence the sizes of autoreactive lymphocyte populations to the greatest extent.

4.3. Linear stability and bifurcation analysis

To further examine the behavior of the reduced model (Eqs. (8) and (9)), we conduct linear stability and bifurcation analysis. The LHS/PRCC analysis results show that the outcome variables, x (scaled level of $CD8^+$ T-cells) and y (scaled level of $CD4^+$ T-cells), are sensitive to changes in the parameters s, a, and b. Exploration of the sensitive parameters reveals that b and a are also bifurcation parameters. So, alterations in b and a cause qualitative changes in the behavior of the dynamical system. More specifically, the bifurcations we observe entail changes in the stability of equilibria.

As we vary the bifurcation parameters, we conduct linear stability analysis to examine the stability of biologically relevant steady states and to classify them. The ranges and baseline values for b and a are as given in Table 5. We vary these parameters one

Biologically relevant equilibrium	Eigenvalues	Classification
$(0,0)$	$\lambda_1 = -0.9487, \lambda_2 = -0.7808$	Stable node

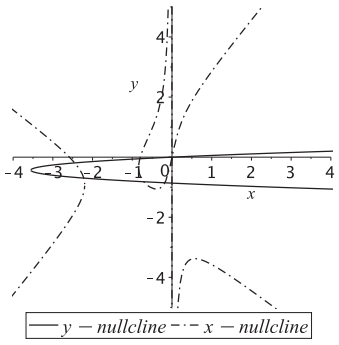

Fig. 7. Nullclines and biologically meaningful steady states for $b=0.0525$.

Biologically relevant equilibrium	Eigenvalues	Classification
$(0,0)$	$\lambda_1 = -0.9888, \lambda_2 = 0.0000$	Transcritical bifurcation

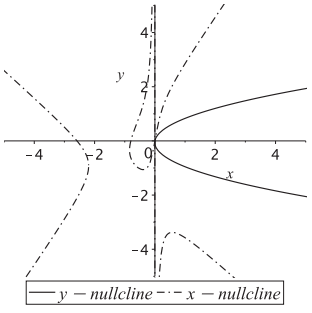

Fig. 8. Nullclines and biologically meaningful steady states for $b=0.79349$.

Biologically relevant equilibrium	Eigenvalues	Classification
$(0,0)$	$\lambda_1 = -0.9979, \lambda_2 = 4.4642$	Saddle point
$(3.4645, 6.9486)$	$\lambda_1 = -2.0113, \lambda_2 = -11.0889$	Stable node

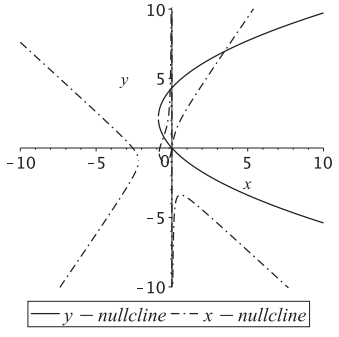

Fig. 9. Nullclines and biologically meaningful steady states for $b=5.25$.

at a time while keeping the remaining parameters at their nominal values. We should also note that only equilibria with non-negative values of x and y carry biological meaning.

The model linearization is given by

$$\begin{pmatrix} \frac{dx}{d\tau} \\ \frac{dy}{d\tau} \end{pmatrix} = J \begin{pmatrix} x \\ y \end{pmatrix}, \tag{10}$$

where J is the Jacobian matrix for the system (Nonlinear Dynamics and Chaos, 2001). In order to find the steady states, (x^*, y^*), we

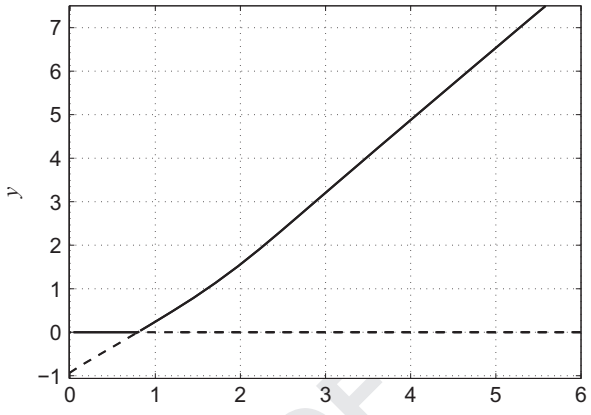

Fig. 10. Bifurcation diagram of scaled level of CD4$^+$ T-cells, y, as a function of b. Transcritical bifurcation at $b=0.79349$. Solid designates stable, and dashed designates unstable. Bifurcation diagram was generated using XPPAUT and Matlab. The bifurcation diagram of x, scaled level of CD8$^+$ T-cells, as a function of b is similar.

Biologically relevant equilibrium	Eigenvalues	Classification
$(0,0)$	$\lambda_1 = -0.9487, \lambda_2 = -0.7808$	Stable node

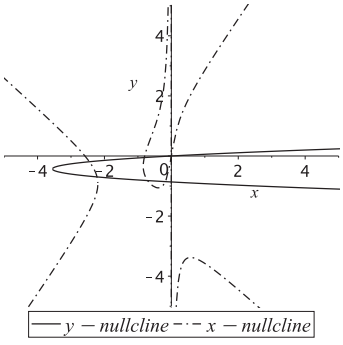

Fig. 11. Nullclines and biologically meaningful steady states for $a=2.3810$.

Biologically relevant equilibrium	Eigenvalues	Classification
$(0,0)$	$\lambda_1 = 0.0000, \lambda_2 = -0.9211$	Transcritical bifurcation

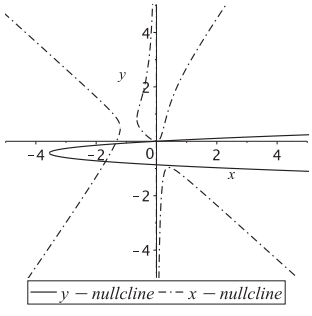

Fig. 12. Nullclines and biologically meaningful steady states for $a=0.33932$.

solve the following equations for x and y:

$$\begin{cases} \frac{v(x+y)}{(1+s)(a+y+x)} + \frac{lxy}{(1+s)} - x - x^2 = 0 \\ \frac{b(x+y)}{(1+s)} + \frac{wy}{(1+s)} - y - y^2 = 0 \end{cases} \tag{11}$$

Then, to determine whether an equilibrium is stable or unstable,

Biologically relevant equilibrium	Eigenvalues	Classification
$(0,0)$	$\lambda_1 = 1.3426 \times 10^3, \lambda_2 = -0.9000$	Saddle point
$(0.2564, 0.0153)$	$\lambda_1 = -1.5158, \lambda_2 = -0.8807$	Stable node

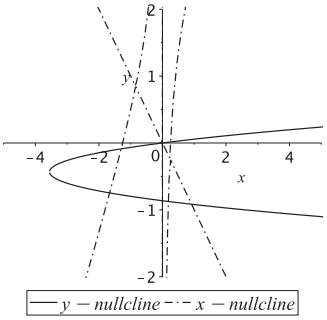

Fig. 13. Nullclines and biologically meaningful steady states for $a = 0.0002381$.

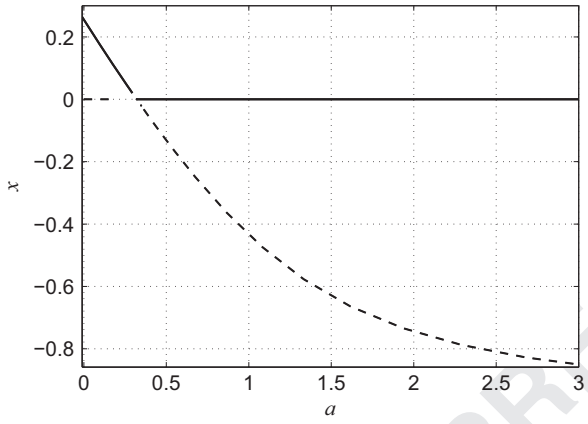

Fig. 14. Bifurcation diagram of scaled level of $CD8^+$ T-cells, x, as a function of a. Transcritical bifurcation at $a = 0.33932$. Solid designates stable, and dashed designates unstable. Bifurcation diagram was generated using XPPAUT and Matlab. The bifurcation diagram of y, scaled level of $CD4^+$ T-cells, as a function of a is similar.

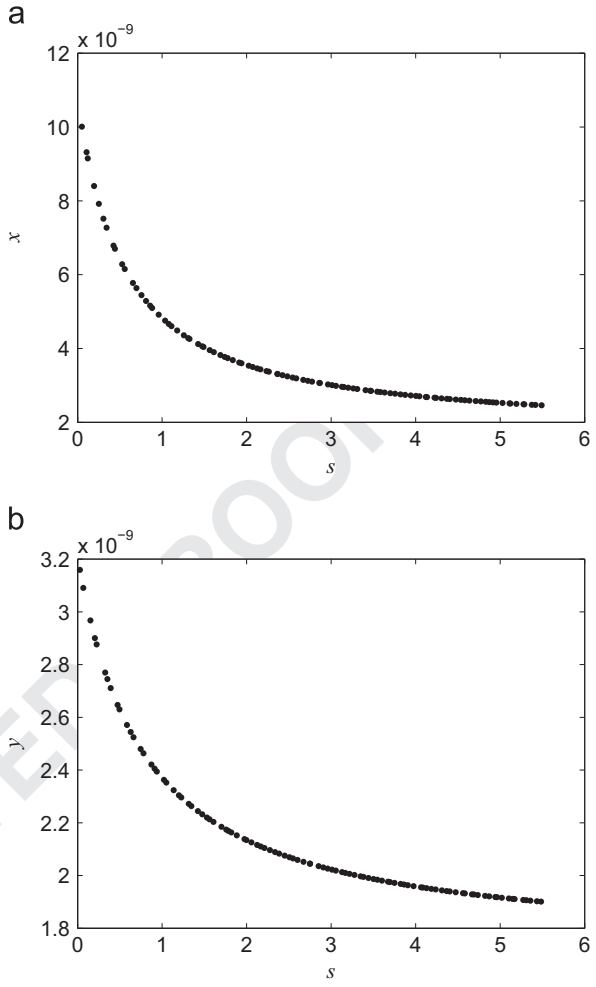

Fig. B1. (a) Scatter plot of the output variable x against the input parameter s. (b) Scatter plot of the output variable y against the input parameter s. The plots confirm that the relationships between s and each outcome variable are monotonic.

we evaluate J at (x^*, y^*) and find the eigenvalues of the Jacobian matrix (Nonlinear Dynamics and Chaos, 2001). In our case, we obtain 2 eigenvalues for each equilibrium since J is a 2×2 matrix. Also, all eigenvalues corresponding to biologically relevant steady states are real. We classify an equilibrium as stable if both eigenvalues corresponding to it are negative. Otherwise, the equilibrium of interest is unstable (Nonlinear Dynamics and Chaos, 2001). We use Matlab in order to perform the linear stability analysis procedure.

First, we examine the qualitative changes brought about by variation in the parameter b. Figs. 7–9 show the phase plane for different values of b. Because b is only in the second equation of the system, alterations in its value change the shape and position of the y-nullcline. As Fig. 10 shows, varying the value of b causes a transcritical bifurcation to occur. The bifurcation point is $b_{critical} = 0.79349$. For $0 \le b < b_{critical}$, we have two equilibria. One of these steady states is (0,0), and it is stable. The other equilibrium is unstable, and it does not carry biological meaning since it occurs at negative values for x and y. When $b = b_{critical}$, (0,0) becomes an equilibrium with a zero eigenvalue. For $b > b_{critical}$, we again have two steady states. The previously unstable equilibrium becomes stable and now occurs at positive values for x and y. On the other hand, (0,0) becomes unstable. As b increases past $b_{critical}$, (0,0) stays unstable, and the positive steady state remains stable.

Since $b = \frac{m\beta g}{d}$, for fixed values of m, β, and d, a large value of b is associated with a high value for the production to degradation ratio of IFN-γ, g. Thus, large b implies elevated IFN-γ level. Also, as pointed out earlier, the diseased state is characterized by large populations of effector autoreactive $CD4^+$ and $CD8^+$ T-cells/$NKG2D^+$ cells in hair follicles, while in the healthy state such cells are absent or present at negligible levels. So, the transcritical bifurcation that occurs signifies hair follicles developing alopecia areata in response to significantly elevated secretion of IFN-γ. As b increases and passes through its critical value of 0.79349, the healthy state loses stability, and the diseased state becomes stable.

Now, we look at the qualitative changes triggered by varying the parameter a. Figs. 11–13 show the phase plane for different values of a. Alterations in a change the shape of the x-nullcline because this parameter appears only in the first equation of the system. As Fig. 14 shows, varying the value of a, results in a transcritical bifurcation. The bifurcation point is $a_{critical} = 0.33932$. For $a > a_{critical}$, we have two steady states. One of these equilibria is at negative values for x and y, and it is unstable. The other equilibrium is (0,0), and it is stable. The unstable steady state to the right of $a_{critical}$ is not biologically meaningful since it occurs at negative values for x and y. When $a = a_{critical}$, (0,0) is a steady state with a zero eigenvalue. For $0 \le a < a_{critical}$, we again have two steady states. (0,0) loses stability, while the previously unstable equilibrium becomes stable and now occurs at positive values for x and y. As a decreases below $a_{critical}$, the positive steady state remains stable, and (0,0) stays unstable.

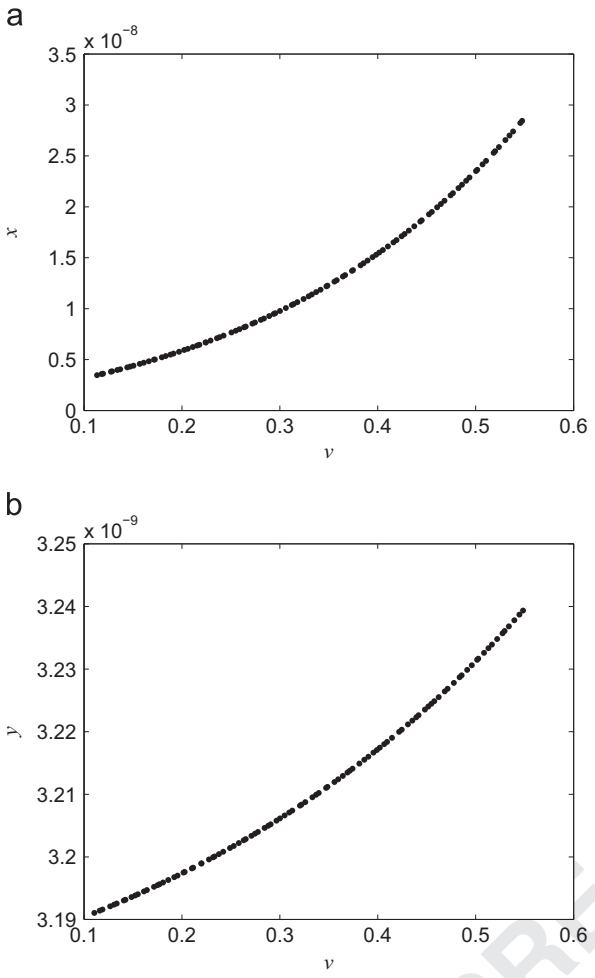

Fig. B2. (a) Scatter plot of the output variable x against the input parameter v. (b) Scatter plot of the output variable y against the input parameter v. The plots confirm that the relationships between v and each outcome variable are monotonic.

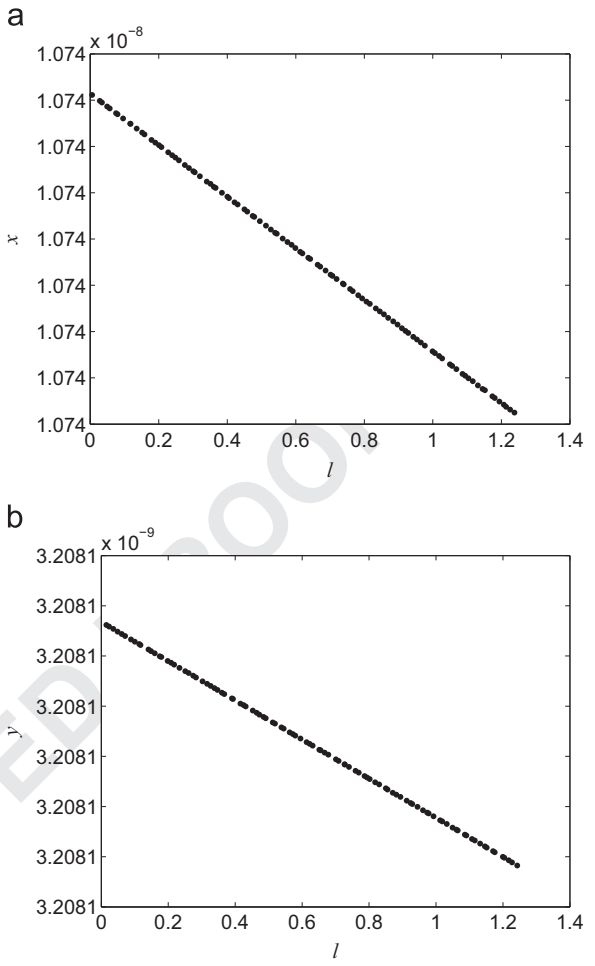

Fig. B3. (a) Scatter plot of the output variable x against the input parameter l. (b) Scatter plot of the output variable y against the input parameter l. The plots confirm that the relationships between l and each outcome variable are monotonic.

Since $a = \frac{r\kappa}{dg}$, for fixed values of r, κ, and d, a low value of a is associated with a large value for g, that is, increased amount of IFN-γ. However, effector autoreactive $CD4_+$ and $CD8_+$ T-cells/$NKG2D^+$ cells do not reach high enough levels to be able to launch a successful cytotoxic attack on hair follicles. This is why, the transcritical bifurcation that occurs as a result of varying a could be interpreted as follicles becoming susceptible to alopecia areata. As mentioned above, all biologically relevant steady states of the system have corresponding eigenvalues that are real. This indicates that disease dynamics, as described by our model, are not associated with oscillatory behavior.

5. Discussion

The mathematical model we develop in this work succeeds in capturing qualitatively two very important processes that are at play in alopecia areata (AA) dynamics: immune privilege guardians and interferon-γ (IFN-γ). Elevated levels of effector autoreactive $CD4^+$ and $CD8^+$ T-cells/$NKG2D^+$ cells penetrating hair follicles are considered indicators of disease. So, in the context of our model, the diseased state entails large populations of effector autoreactive $CD4^+$ and $CD8^+$ T-cells/$NKG2D^+$ cells, while the healthy state is characterized by the absence or negligible presence of such cells. In accordance with the immune privilege collapse hypothesis for AA pathogenesis, the model predicts that significant increase in the amount of IFN-γ leads to high numbers of autoreactive $CD4^+$ and $CD8^+$ T-cells/$NKG2D^+$ cells that cause damage to hair follicles. So, hair follicles become diseased with AA in response to elevated secretion of IFN-γ. In addition, the model is predictive of the influence of immune privilege guardians: sufficient amount of potent immune privilege guardians brings the sizes of effector autoreactive T-cell populations down to a very low level at which a detrimental autoimmune response against hair follicles cannot occur. Thus, hair follicles remain healthy as long as they produce enough immune privilege agents that can keep pro-inflammatory events in check.

More leukocytes, such as mast cells and regulatory T-cells, have been shown to play a role in AA (McElwee et al., 2013; Gilhar et al., 2007). However, we refrained from incorporating these leukocytes for the purpose of constructing a model that is both qualitatively consistent with AA dynamics and simpler to interpret and analyze. Exploring the participation of other cellular players is certainly important, and they could be made part of future models. Although, a key conclusion from the model established in this study is that cytokines and immune privilege agents have much stronger effect on disease development and recovery than cellular dynamics. This result could also be useful in directing the investigation of therapeutic strategies toward alternatives with the highest potential impact.

In addition, our hope is that the model can help to explain what happens at the early stages of the disease, even before a hairless patch has formed. We believe this is essential for a better

Please cite this article as: Dobreva, A., et al., Mathematical model for alopecia areata. J. Theor. Biol. (2015), http://dx.doi.org/10.1016/j.jtbi.2015.05.033

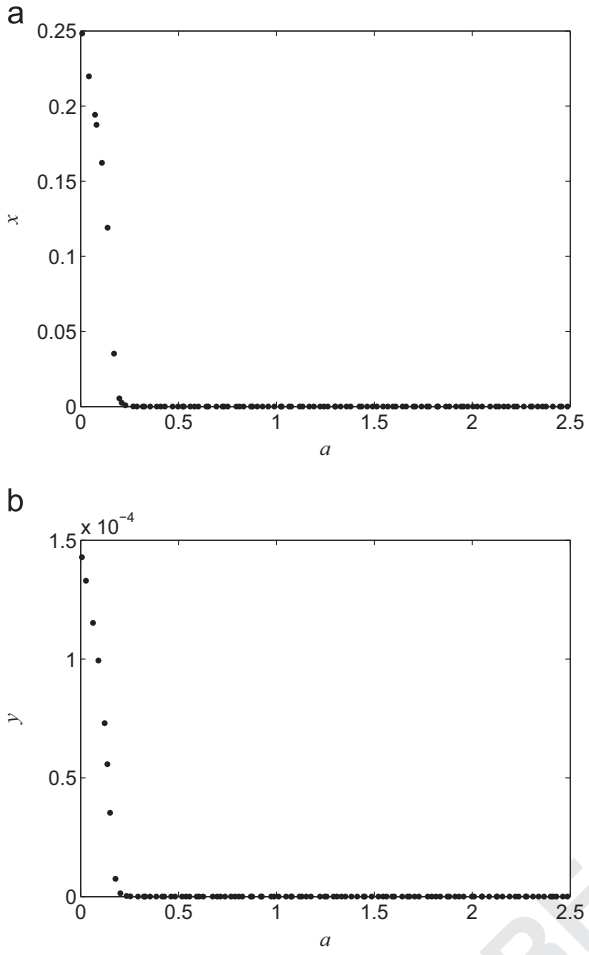

Fig. B4. (a) Scatter plot of the output variable x against the input parameter a. (b) Scatter plot of the output variable y against the input parameter a. The plots confirm that the relationships between a and each outcome variable are monotonic.

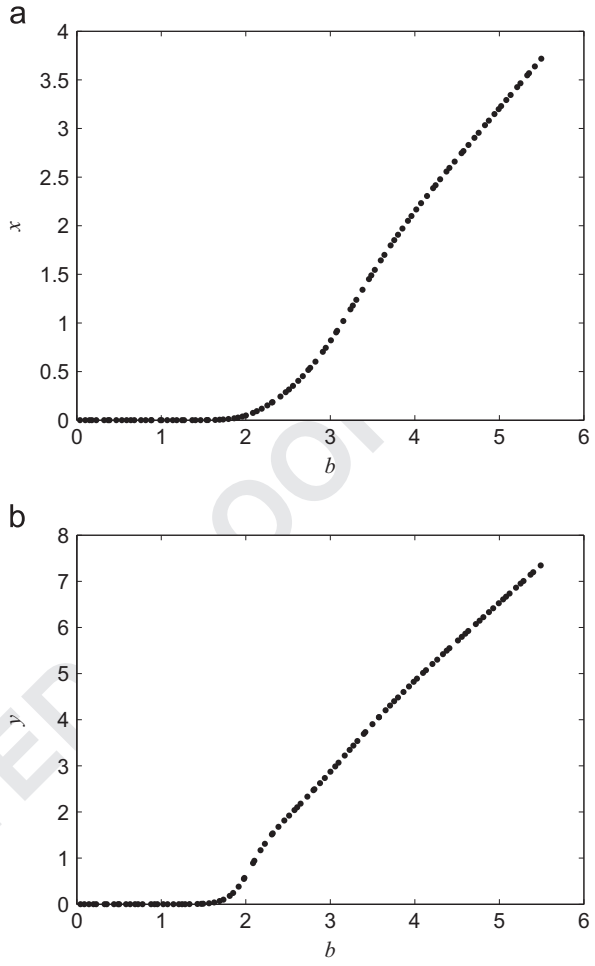

Fig. B5. (a) Scatter plot of the output variable x against the input parameter b. (b) Scatter plot of the output variable y against the input parameter b. The plots confirm that the relationships between b and each outcome variable are monotonic.

understanding of AA and will help in the development of more effective treatments. What is currently known about the disease comes from information collected after patches have already appeared and have been noticed. So, clinicians and scientists do not have a firm grasp of what happens in hair follicles and with the cells and signals of the immune system as an AA-lesion is about to emerge. Our model could help to fill this gap and make it possible to test hypothetical scenarios in order to obtain clarity on unresolved questions regarding the pathogenesis of the disease. This would not only contribute to a better understanding of AA, but it will also aid in the broader investigation of the mechanisms of immune privilege and autoimmunity.

Appendix A. Model reduction process

The rates of cytokine secretion, receptor binding and degradation are much larger than the rates at which cells migrate, get activated, proliferate, and die (Yates et al., 2000; Lortat-Jacob et al., 1996; Akdis et al., 1995; Ashton et al., 1977; Kirschner, 1999; Mohri et al., 2001; Schiller et al., 2004). Also, peptide–MHC I complex formation, receptor binding, and decay occur faster than lymphocyte dynamics (Mohri et al., 2001; Princiotta et al., 2003; Ackerman and Cresswell, 2003). These observations allow us to make a quasi-steady state assumption for IPG, IFN, and MI and set $\frac{dIPG}{dt}=0$, $\frac{dIFN}{dt}=0$, and $\frac{dMI}{dt}=0$.

Applying the assumption, we obtain

$$\frac{dT8}{dt}=m_{T8}\frac{\alpha MI}{1+\sigma IPG}+\frac{p_{T8}\gamma T4T8}{1+\sigma IPG}-d_{T8}T8-\kappa_{T8}(T8)^2 \tag{A.1}$$

$$\frac{dT4}{dt}=m_{T4}\frac{\beta IFN}{1+\sigma IPG}+\frac{p_{T4}T4}{1+\sigma IPG}-d_{T4}T4-\kappa_{T4}(T4)^2 \tag{A.2}$$

where

$$IPG=\frac{p_{IPG}}{d_{IPG}}=c \tag{A.3}$$

$$IFN=\frac{p_{IFN}}{d_{IFN}}(T4+T8)=g(T4+T8) \tag{A.4}$$

$$MI=\frac{p_{MI}}{d_{MI}}\left(\frac{IFN}{r+IFN}\right)=\frac{p_{MI}}{d_{MI}}\left(\frac{\frac{p_{IFN}}{d_{IFN}}(T4+T8)}{r+\frac{p_{IFN}}{d_{IFN}}(T4+T8)}\right)$$
$$=\mu\left(\frac{g(T4+T8)}{r+g(T4+T8)}\right). \tag{A.5}$$

For simplicity, we assume that $CD4^+$ and $CD8^+$ T-cells/$NKG2D^+$ cells have comparable rates of migration, proliferation, death, and concentration-dependent death, that is

- $m_{T8}=m_{T4}=m$
- $p_{T8}=p_{T4}=p$
- $d_{T8}=d_{T4}=d$

Please cite this article as: Dobreva, A., et al., Mathematical model for alopecia areata. J. Theor. Biol. (2015), http://dx.doi.org/10.1016/j.jtbi.2015.05.033

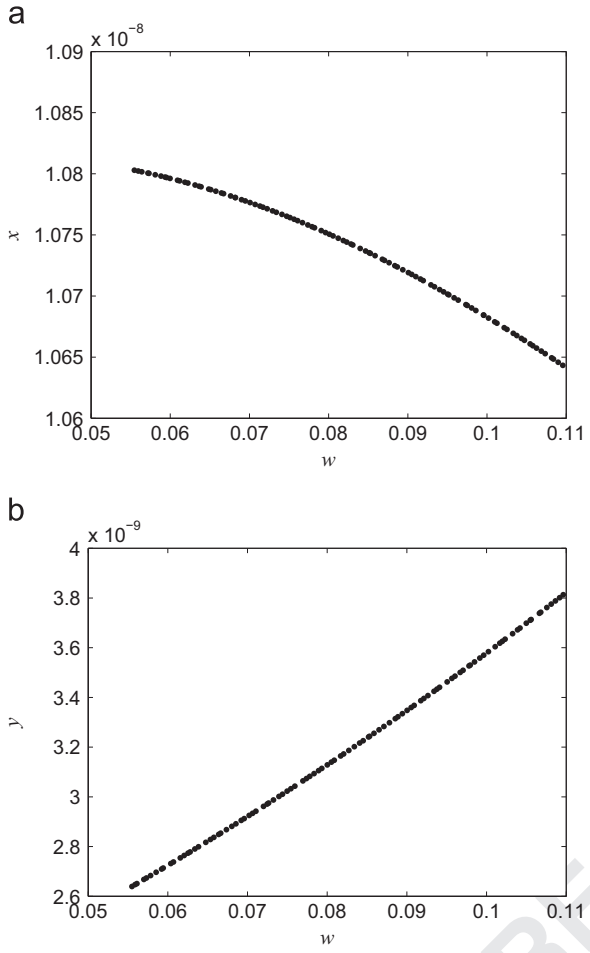

Fig. B6. (a) Scatter plot of the output variable x against the input parameter w. (b) Scatter plot of the output variable y against the input parameter w. The plots confirm that the relationships between w and each outcome variable are monotonic.

- $\kappa_{T8} = \kappa_{T4} = \kappa$.

Using this assumption and substituting in the expressions for *IPG*, *IFN*, and *MI*, the system becomes

$$\frac{dT8}{dt} = \frac{m\alpha\mu}{1+\sigma c}\left(\frac{g(T4+T8)}{r+g(T4+T8)}\right) + \frac{p\gamma T4T8}{1+\sigma c} - dT8 - \kappa(T8)^2 \tag{A.6}$$

$$\frac{dT4}{dt} = \frac{m\beta g(T4+T8)}{1+\sigma c} + \frac{pT4}{1+\sigma c} - dT4 - \kappa(T4)^2. \tag{A.7}$$

Next, we express the variables $T8$, $T4$, and t as $T8 = x\hat{x}$, $T4 = y\hat{y}$, $t = \tau\hat{t}$ where x, y, and τ are dimensionless variables, and $\hat{x}$, $\hat{y}$, and $\hat{t}$ carry the units associated with $T8$, $T4$, and t, respectively

$$\frac{d(x\hat{x})}{d(\tau\hat{t})} = \frac{m\alpha\mu}{1+\sigma c}\left(\frac{g(y\hat{y}+x\hat{x})}{r+g(y\hat{y}+x\hat{x})}\right) + \frac{p\gamma(y\hat{y})(x\hat{x})}{1+\sigma c} - d(x\hat{x}) - \kappa(x\hat{x})^2 \tag{A.8}$$

$$\frac{d(y\hat{y})}{(\tau\hat{t})} = \frac{m\beta g(y\hat{y}+x\hat{x})}{1+\sigma c} + \frac{p(y\hat{y})}{1+\sigma c} - d(y\hat{y}) - \kappa(y\hat{y})^2. \tag{A.9}$$

Simplifying, we obtain

$$\frac{dx}{d\tau} = \frac{\hat{t}m\alpha\mu gx}{(1+\sigma c)(r+gy\hat{y}+gx\hat{x})} + \frac{\hat{t}m\alpha\mu gy\hat{y}}{\hat{x}(1+\sigma c)(r+gy\hat{y}+gx\hat{x})} + \frac{\hat{t}p\gamma y\hat{y}x}{1+\sigma c} - \hat{t}dx - \hat{t}\hat{x}\kappa x^2 \tag{A.10}$$

$$\frac{dy}{d\tau} = \frac{\hat{t}m\beta gx\hat{x}}{\hat{y}(1+\sigma c)} + \frac{\hat{t}m\beta gy}{1+\sigma c} + \frac{\hat{t}py}{1+\sigma c} - \hat{t}dy - \hat{t}\hat{y}\kappa y^2. \tag{A.11}$$

Choosing $\hat{x} = \hat{y} = \frac{d}{\kappa}$, $\hat{t} = \frac{1}{d}$, we get

$$\frac{dx}{d\tau} = \frac{m\alpha\mu gx}{d(1+\sigma c)\left(r+\frac{gd}{\kappa}y+\frac{gd}{\kappa}x\right)} + \frac{m\alpha\mu gy}{d(1+\sigma c)\left(r+\frac{gd}{\kappa}y+\frac{gd}{\kappa}x\right)} + \frac{p\gamma xy}{\kappa(1+\sigma c)} - x - x^2 \tag{A.12}$$

$$\frac{dy}{d\tau} = \frac{m\beta gx}{d(1+\sigma c)} + \frac{m\beta gy}{d(1+\sigma c)} + \frac{py}{d(1+\sigma c)} - y - y^2. \tag{A.13}$$

Finally, we rewrite the above equations as

$$\frac{dx}{d\tau} = \frac{v(x+y)}{(1+s)(a+y+x)} + \frac{lxy}{(1+s)} - x - x^2 \tag{A.14}$$

$$\frac{dy}{d\tau} = \frac{b(x+y)}{(1+s)} + \frac{wy}{(1+s)} - y - y^2 \tag{A.15}$$

where we have the following dimensionless parameters:

- $s = \sigma c$
- $v = \frac{m\alpha\mu\kappa}{d^2}$
- $l = \frac{p\gamma}{\kappa}$
- $a = \frac{r\kappa}{gd}$
- $b = \frac{m\beta g}{d}$
- $w = \frac{p}{d}$

Appendix B. Monotonicity plots

The scatter plots shown in this appendix were created to examine the nature of the input-output relationships in the reduced model. Parameters were varied one at a time according to a procedure explained in Marino et al. (2008) and Blower and Dowlatabadi (1994). The output values of x and y at $\tau = 10$ were plotted against the changes in each input parameter (see Figs. B1–B6).

References

Ackerman, A.L., Cresswell, P., 2003. Regulation of MHC class I transport in human dendritic cells and the dendritic-like cell line KG-1. J. Immunol. 170, 4178–4188.

Akdiş, A.C., Towbin, H., Libsig, P., Motz, J., Alkan, Ş.Ş., 1995. Cytokine immunotrapping: an assay to study the kinetics of production and consumption or degradation of human interferon-γ. J. Immunol. Methods 182, 251–261.

Alkhalifah, A., Alsantali, A., Wang, E., McElwee, K.J., Shapiro, J., 2010a. Alopecia areata update: Part I. Clinical picture, histopathology, and pathogenesis. J. Am. Acad. Dermatol. 62, 177–188.

Alkhalifah, A., Alsantali, A., Wang, E., McElwee, K.J., Shapiro, J., 2010b. Alopecia areata update: Part II. Treatment. J. Am. Acad. Dermatol. 62, 191–202.

Alli, R., Nguyen, P., Boyd, K., Sundberg, J.P., Geiger, T.L., 2012. A mouse model of clonal CD8+ T lymphocyte-mediated alopecia areata progressing to alopecia universalis. J. Immunol. 188 (1), 477–486.

Al-Nuaimi, Y., Baier, G., Watson, R.E.B., Chuong, C.-M., Paus, R., 2010. The cycling hair follicle as an ideal systems biology research model. Exp. Dermatol. 19, 707–713.

Al-Nuaimi, Y., Goodfellow, M., Paus, R., Baier, G., 2012. A prototypic mathematical model of the human hair cycle. J. Theoret. Biol. 310, 143–159.

Ashton, H., Millman, J.E., Telford, R., Thompson, J.W., Davies, T.F., Hall, R., Shuster, S., Thody, A.J., Coy, D.H., Kastin, A.J., 1977. Psychopharmacological and endocrinological effects of melanocyte stimulating hormones in normal man. Psychopharmacology 55 (2), 165–172.

Bergfeld, W.F., Mulinari-Brenner, F., 2001. Shedding: how to manage a common cause of hair loss. Clevel. Clin. J. Med. 68 (3), 256–261.

Blower, S.M., Dowlatabadi, H., 1994. Sensitivity and uncertainty analysis of com680 plex models of disease transmission: an HIV model, as an example. Int. Stat. Rev. 62 (2), 229–243.

Borghans, J.A.M., Boer, R.J.D., Sercarz, E., Kumar, V., 1998. T cell vaccination in experimental autoimmune encephalomyelitis: a mathematical model. J. Immunol. 161, 1087–1093.

Catanzaro, D., Andrien, M., Labbé, M., Toungouz-Nevessignsky, M., 2010. Computer-aided human leukocyte antigen association studies: a case study for psoriasis and severe alopecia areata. Human Immunol. 71, 783–788.

Eicheler, W., Happle, R., Hoffmann, R., 1998. 5α-Reductase activity in the human hair follicle concentrates in the dermal papilla. Arch. Dermatol. Res. 290, 126–132.

Freyschmidt-Paul, P., McElwee, K.J., Hoffmann, R., Sundbergn, J.P., Vitacolonna, M., Kissling, S., Zöler, M., 2006. Interferon-γ-deficient mice are resistant to the development of alopecia areata. Br. J. Dermatol. 155, 515–521.

Gilhar, A., 2010. Collapse of immune privilege in alopecia areatacoincidental or substantial?. J. Invest. Dermatol. 130, 2535–2537.

Gilhar, A., Ullmann, Y., Berkutzki, T., Assy, B., Kalish, R.S., 1998. Autoimmune hair loss (alopecia areata) transferred by T lymphocytes to human scalp explants on SCID mice. J. Clin. Invest. 101 (1), 62–67.

Gilhar, A., Landau, M., Assy, B., Shalaginov, R., Serafimovich, S., Kalish, R.S., 2002. Mediation of alopecia areata by cooperation between $CD4^+$ and $CD8^+$ T lymphocytes: transfer to human scalp explants on $Prkdc^{scid}$ mice. Arch. Dermatol. 138 (7), 916–922.

Gilhar, A., Paus, R., Kalish, R.S., 2007. Lymphocytes, neuropeptides, and genes involved in alopecia areata. J. Clin. Invest. 117, 2019–2027.

Gilhar, A., Etzioni, A., Paus, R., 2012. Medical progress: alopecia areata. N. Eng. J. Med. 366 (16), 1515–1525.

Giordano, C.N., Sinha, A.A., 2013. Cytokine pathways and interactions in alopecia areata. Eur. J. Dermatol. 23 (3), 308–318.

Hajheydari, Z., Jamshidi, M., Akbari, J., Mohammadpour, R., 2007. Combination of topical garlic gel and betamethasone valerate cream in the treatment of localized alopecia areataa double-blind randomized controlled study. Indian J. Dermatol. Venereol. Leprol. 73 (1), 29–32.

Halloy, J., Bernard, B.A., Loussouarn, G., Goldbeter, A., 2000. Modeling the dynamics of human hair cycles by a follicular automaton. Proc. Natl. Acad. Sci. 97 (15), 8328–8333.

Halloy, J., Bernard, B.A., Loussouarn, G., Goldbeter, A., 2002. The follicular automaton model: effect of stochasticity and of synchronization of hair cycles. J. Theoret. Biol. 214, 469–479.

Ito, T., 2010. Hair follicle is a target of stress hormone and autoimmune reactions. J. Dermatol. Sci. 60, 67–73.

Ito, T., 2013. Recent advances in the pathogenesis of autoimmune hair loss disease alopecia areata. Clin. Dev. Immunol. 2013, 1–6.

Ito, T., Ito, N., Bettermann, A., Tokura, Y., Takigawa, M., Paus, R., 2004. Collapse and restoration of MHC Class-I-dependent immune privilege. Am. J. Pathol. 164 (2), 623–634.

Ito, T., Ito, N., Saathoff, M., Bettermann, A., Takigawa, M., Paus, R., 2005. Interferon-$\gamma$is a potent inducer of catagen-like changes in cultured human anagen hair follicles. Br. J. Dermatol. 152, 623–631.

Kageyama, S., Tsomides, T.J., Sykulev, Y., Eisen, H.N., 1995. Variations in the number of peptide-MHC Class I complexes required to activate cytotoxic T cell responses. J. Immunol. 154, 567–576.

Kalabokes, V.D., 2011. Alopecia areata: support groups and meetings—how can it help your patient? Dermatol. Therapy 24, 302–304.

Kirschner, D., 1999. Dynamics of co-infection with M. tuberculosis and HIV-1. Theoret. Popul. Biol. 55, 94–109.

Kutner, A., Friedman, A., 2013. Hair loss in the dermatology office: an update on alopecia areata. J. Drugs Dermatol. 12 (5), 588–593.

Lortat-Jacob, H., Baltzer, F., Grimaud, J., 1996. Heparin decreases the blood clearance of interferon-$\gamma$and increases its activity by limiting the processing of its carboxyl-terminal sequence. J. Biol. Chem. 271 (27), 16139–16143.

Marino, S., Hogue, I.B., Ray, C.J., Kirschner, D.E., 2008. A methodology for performing global uncertainty and sensitivity analysis in systems biology. J. Theoret. Biol. 254 (1), 178–196.

McElwee, K.J., Hoffmann, R., Freyschmidt-Paul, P., Wenzel, E., Kissling, S., Sundberg, J.P., Zöller, M., 2002. Resistance to alopecia areata in C3H/HeJ mice is associated with increased expression of regulatory cytokines and a failure to recruit $CD4^+$ and $CD8^+$ cells. J. Invest. Dermatol. 119, 1426–1433.

McElwee, K.J., Freyschmidt-Paul, P., Sundbergn, J.P., Hoffmann, R., 2003. The pathogenesis of alopecia areata in rodent models. JID Symp. Proc. 8, 6–11.

McElwee, K.J., Gilhar, A., Tobin, D.J., Ramot, Y., Sundberg, J.P., Nakamura, M., Bertolini, M., Inui, S., Tokura, Y., Jr, L.E.K., Duque-Estrada, B., Tosti, A., Keren, A., Itami, S., Shoenfeld, Y., Zlotogorski, A., Paus, R., 2013. What causes alopecia areata? Exp. Dermatol. 22, 609–626. Q4

Millar, S.E., 2002. Molecular mechanisms regulating hair follicle development. J. Invest. Dermatol. 118 (2), 216–225.

Mohri, H., Perelson, A.S., Tung, K., Ribeiro, R.M., Ramratnam, B., Markowitz, M., Kost, R., Hurley, A., Weinberger, L., Cesar, D., Hellerstein, M.K., Ho, D.D., 2001. Increased turnover of T lymphocytes in HIV-1 infection and its reduction by antiretroviral therapy. J. Exp. Med 194 (9), 1277–1287.

Murray, P.J., Maini, P.K., Plikus, M.V., Chuong, C.-M., Baker, R.E., 2012. Modelling hair follicle growth dynamics as an excitable medium. PLOS Comput. Biol. 8 (12), e1002804.

Nicholson, D., Kerr, E.C., Jepps, O.G., Nicholson, L.B., 2012. Modelling experimental uveitis: barrier effects in autoimmune disease. Inflam. Res. 61, 759–773.

Paus, R., Cotsarelis, G., 1999. The biology of hair follicles. N. Eng. J. Med. 341 (7), 491–497.

Paus, R., Slominski, A., Czametzki, B.M., 1994. Is alopecia areata an autoimmune-response against melanogenesis-related proteins, exposed by abnormal MHC class I expression in the anagen hair bulb. Yale J. Biol. Med. 66, 541–554.

Paus, R., Ito, N., Takigawa, M., Ito, T., 2003. The hair follicle and immune privilege. JID Symp. Proc. 8 (2), 188–194.

Paus, R., Nickoloff, B.J., Ito, T., 2005. A 'hairy' privilege. TRENDS Immunol. 26 (1), 32–40.

Paus, R., Arck, P., Tiedea, S., 2008. (Neuro-)endocrinology of epithelial hair follicle stem cells. Mol. Cell. Endocrinol. 288, 38–51.

Princiotta, M.F., Finzi, D., Qian, S., Gibbs, J., Schuchmann, S., Buttgereit, F., Bennink, J. R., Yewdell, J.W., 2003. Quantitating protein synthesis, degradation, and endogenous antigen processing. Immunity 18, 343–354.

Rivitti, E.A., 2005. Alopecia areata: a revision and update. An. Bras. Dermatol. 80 (1), 57–68.

Schiller, M., Brzoska, T., Böhm, M., Metze, D., Scholzen, T.E., Rougier, A., Luger, T.A., 2004. Solar-simulated ultraviolet radiation-induced upregulation of the melanocortin-1 receptor, proopiomelanocortin, and α-melanocyte-stimulating hormone in human epidermis in vivo. J. Invest. Dermatol. 122, 468–476.

Schodin, B.A., Tsomides, T.J., Kranz, D.M., 1996. Correlation between the number of T cell receptors required for T cell activation and TCR-ligand affinity. Immunity 5, 137–146.

Segel, L.A., Jäger, E., Elias, D., Cohen, I.R., 1995. A quantitative model of autoimmune disease and T-cell vaccination: does more mean less?. Immunol. Today 16 (2), 80–84.

Sun, J., Silva, K.A., McElwee, K.J., Jr, L.E.K., Sundbergn, J.P., 2008. The C3H/HeJ mouse and DEBR rat models for alopecia areatareview of preclinical drug screening approaches and results. Exp. Dermatol. 17, 793–805.

Yang, I., Kremen, T.J., Giovannone, A.J., Paik, E., Odesa, S.K., Prins, R.M., Liau, L.M., 2004. Modulation of major histocompatibility complex class I molecules and major histocompatibility complex-bound immunogenic peptides induced by interferon-$\alpha$and interferon-γtreatment of human glioblastoma multiforme. J. Neurosurg. 100, 310–319.

Yates, A., Bergmann, C., Hemmen, J.L.V., Stark, J., Callard, R., 2000. Cytokine-modulated regulation of helper T cell populations. J. Theoret. Biol. 206, 539–560.

Zhao, Y., Zhang, B., Caulloo, S., Chen, X., Li, X.Z.Y., 2012. Diffuse alopecia areata is associated with intense inflammatory infiltration and CD8+ T cells in hair loss regions and an increase in serum IgE level. Indian J. Dermatol. Venereol. Leprol. 78 (6), 709–714.

2001. Phase plane. In: Nonlinear Dynamics and Chaos: With Applications to Physics, Biology, Chemistry, and Engineering, Westview Press. Q5

Please cite this article as: Dobreva, A., et al., Mathematical model for alopecia areata. J. Theor. Biol. (2015), http://dx.doi.org/10.1016/j.jtbi.2015.05.033